Journal of Power Sources 183 (2008) 792–798

Contents lists available at ScienceDirect

Journal of Power Sources

journal homepage: www.elsevier.com/locate/jpowsour

Influence of acceptor moiety in triphenylamine-based dyes on the properties of dye-sensitized solar cells

Wei Xu, Juan Pei, Jifu Shi, Shengjie Peng, Jun Chen *

Institute of New Energy Material Chemistry, Key Laboratory of Energy-Material Chemistry (Tianjin) and Engineering Research Center of Energy Storage & Conversion (Ministry of Education), Chemistry College, Nankai University, Tianjin 300071, People's Republic of China

ARTICLE INFO

Article history:
Received 5 March 2008
Received in revised form 8 May 2008
Accepted 8 May 2008
Available online 16 May 2008

Keywords:
Dye-sensitized solar cell
Triphenylamine-based dye
Acceptor moiety
Coadsorbent
Light-to-electricity conversion efficiency

ABSTRACT

Triphenylamine-based organic dyes with different acceptor parts have been synthesized in an attempt to investigate the effect of the acceptor moiety on the properties of dye-sensitized solar cells. The light-to-electricity conversion efficiencies of 4.67% and 5.05% were obtained for the DSCs based on 2-(4-oxo-5-(4-(phenyl(4-styrylphenyl)amino)benzylidene)-2-thioxothiazolidin-3-yl)acetic acid (TPAR11) and 2-cyano-3-(4-(phenyl(4-styrylphenyl)amino)phenyl)acrylic acid (TC12), respectively. A molecular-orbital calculation shows that the delocalization of the excited state for TPAR11 is broken between the 4-oxo-2-thioxothiazolidine ring and the acetic acid, which affects the electron movement from dye molecule to the semiconductor film. The effects of chenodeoxycholic acid (CDCA) as the coadsorbent on the photovoltaic performance of the DSCs based on TPAR11 and TC12 have been also studied. It has been found that the addition of 1 mM CDCA coadsorbent improves the photocurrent for TPAR11 and the photovoltage for TC12, owing to the suppression of the quenching processes of the excited electrons between dye molecules or/and a more negative conductive band edge of TiO_2 film. With the addition of 1 mM CDCA, the light-to-electricity conversion efficiencies of the DSCs based on TPAR11 and TC12 were 5.46% and 5.96%, respectively. This result indicates that both the acceptor moiety of metal-free organic dyes and the coadsorbent added in the electrode preparation have the effect on the photovoltaic performance of DSCs.

1. Introduction

Dye-sensitized solar cells (DSCs) have attracted more and more attention because of their high photoelectric conversion efficiency and low cost [1]. The performance of DSCs is mainly affected by anode with semiconductor, cathode with catalyst, electrolyte with redox species and photosensitive dyes [2–5]. As a key part of DSCs, the dyes can absorb the appropriate light and inject the photo-excited electrons to the conduction band of the semiconductor in the anode. Up to now, DSCs based on Ru-complex photosensitizers have exhibited the highest photo-to-current conversion efficiency and long-term chemical stability [6], while metal-free organic dyes have also been concerned due to their low cost [7,8].

Generally, metal-free organic dyes possess the evident molecular structure of the donor part and the acceptor part bridged by the conjugated chain. As a class of the donor part, triphenylamine (TPA) and its derivatives have shown promising applications in the development of photovoltaic devices [9,10]. As the excited electrons on the dye molecules are injected to the semiconductor film through the acceptor moiety [11], the acceptor part has significant influence on the photovoltaic properties of the dyes. For example, Ito et al. employed rhodanine-3-acetic acid as the acceptor on indoline-based dye and attained the overall conversion efficiency of 9.03%, which was the highest value among the metal-free organic dyes so far [12]. Hara et al. used cyanoacrylic acid as the acceptor on coumarin-based dyes to investigate the influence of the different donor parts and got the overall efficiency range from 3.1% to 7.7% [13,14]. Recently, our group has reported a serial of TPA-based organic dyes, showing that extending the π-conjugation of the donor part could improve the photovoltaic performance of the DSCs [15,16].

On the other hand, much processing effort has also been made to improve the photovoltaic performance of DSCs such as open-circuit photovoltage (V_{oc}), short-circuit photocurrent (J_{sc}), fill factor (ff) and overall light-to-electricity conversion efficiency (η) [17]. For example, treating the titania surface with agents such as 4-*tert*-butylpyridine (TBP) or ammonia can produce an increase in V_{oc}, but generally accompanied with a significant drop in photocurrent [18]. While coadsorbing deoxycholic acid (DCA) or guanidine acid can improve both of them [19]. With the similar structure of cholesterol-based molecule to DCA, chenodeoxycholic acid (CDCA) was also used as the coadsorbent to improve the performance of

* Corresponding author. Fax: +86 22 23506808.
E-mail address: chenabc@nankai.edu.cn (J. Chen).

0378-7753/$ – see front matter © 2008 Elsevier B.V. All rights reserved.
doi:10.1016/j.jpowsour.2008.05.025

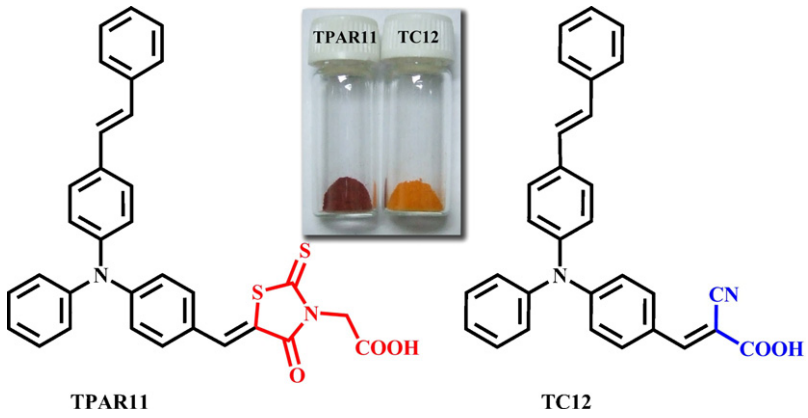

Fig. 1. Molecular structure of the two triphenylamine-based dyes (TPAR11 and TC12). The different acceptor parts have been marked by color drawing. Inset image is the powder photograph of the as-synthesized dyes (in glass bottles).

the device [20]. However, to the best of our knowledge, the influence of CDCA on the different acceptor parts in V_{oc} and J_{sc} has not been reported yet.

Herein, we design and synthesize two novel organic dyes (TPAR11 and TC12) containing styryl triphenylamine as the donor part and rhodanine-3-acetic acid or cyanoacrylic acid as the electron acceptor (Fig. 1). The influence of two different acceptor moieties on the optical and electrochemical characters of the dyes and the performances of the DSCs were studied. Theoretical calculation shows that the delocalization of the excited state for TPAR11 is broken between the 4-oxo-2-thioxothiazolidine ring and the acetic acid, affecting the transfer of electrons from dye molecule to the semiconductor film. To improve the performance of the cells based on these two dyes, CDCA was used as a coadsorbent. In particular, electrochemical impedance spectroscopy (EIS) was employed to scrutinize the salient factors of CDCA governing the performance of DSCs. The results have shown that the presence of the coadsorbent of CDCA resulted in the shifting of the band edges of TiO_2 to negative potentials and the shielding of the surface against recombination.

2. Experimental

2.1. Synthesis of the dyes

Two dyes based on styryl triphenylamine (TPAR11 and TC12) were synthesized by Knoevenagel condensation reaction of the styryl triphenylamine aldehyde and rhodanine-3-acetic acid or cyanoacrylic acid. The styryl triphenylamine aldehyde was prepared from 4,4′-(phenylazanediyl)dibenzaldehyde and benzyltriphosphonium bromide by Wittig reaction. The starting material 4,4′-(phenylazanediyl)dibenzaldehyde was prepared by treating triphenylamine with $POCl_3$ in dimethyl formamide (DMF) according to literature procedure [21].

2.1.1. 4-(Phenyl(4-styrylphenyl)amino)benzaldehyde (**1**)

To a solution of 9.9 mmol (4.3 g) of benzyltriphosphonium bromide in 60 mL dry THF, 10 mmol (1.12 g) potassium *tert*-butylate was added under cooling in nitrogen atmosphere. After stirred for half an hour at room temperature, the solution was added into 30 mL THF with 6.64 mmol (2 g) 4,4′-(phenylazanediyl)dibenzaldehyde slowly, and stirred for further 5 h. Then the solution was washed by distilled water and extracted by ether. The organic phase was dried by anhydrous sodium sulfate, and purified by column chromatography over a silica-gel column with petrol ether/acetic acid as eluent, resulting 1.04 g of yellow **1** in 41.8% yield. TPAR11: ^{1}H NMR (300 MHz, DMSO-d_6) δ (ppm): 9.77 (1H, d), 7.73 (2H, q), 7.62 (2H, *t*), 7.46–7.35 (3H, m), 7.29–7.14 (9H, m), 7.04 (1H, d), 6.92 (2H, q), 6.62 (1H, d). ESI-MS: *m*/*z* 374 ([M−H]$^-$).

2.1.2. 2-(4-Oxo-5-(4-(phenyl(4-styrylphenyl)amino)-benzylidene)-2-thioxothiazolidin-3-yl)acetic acid (TPAR11)

1 (300 mg, 0.8 m mol) and rhodanine-3-acetic acid (171 mg, 0.9 mmol) were added into 15 mL glacial acetic acid and refluxed for 3 h in the presence of 100 mg ammonium acetate. After cooling to room temperature, the mixture was poured into ice water. The precipitate was filtered, washed by distilled water, dried under vacuum, and purified by column chromatography (ethyl acetate/ethanol), resulting in red powder of TPAR11 (342 mg, 78.0%). ^{1}H NMR (300 MHz, DMSO-d_6) δ (ppm): 7.67 (1H, s), 7.60 (3H, *t*), 7.51 (2H, d), 7.45–7.35 (4H, m), 7.29–7.11 (9H, m), 6.98 (2H, m), 4.43 (2H, s). ESI-MS: *m*/*z* 547 ([M−H]$^-$).

2.1.3. 2-Cyano-3-(4-(phenyl(4-styrylphenyl)amino)-phenyl)acrylic acid (TC12)

Same as TPAR11 but 2-cyanoacetic acid (85 mg, 1 mmol) instead of rhodanine-3-acetic acid was used, resulting in dark orange powder (265 mg, 74.9%). ^{1}H NMR (300 MHz, DMSO-d_6) δ (ppm): 7.91 (1H, s), 7.80 (3H, *t*), 7.60 (2H, d), 7.43–7.35 (4H, m), 7.28–7.10 (9H, m), 6.96 (2H, m). ESI-MS: *m*/*z* 441 ([M−H]$^-$).

2.2. Analytical measurements

^{1}H nuclear magnetic resonance (NMR) spectra of the as-prepared dyes were carried out with a Varian Mercury V × 300 spectrometer at 300 MHz with the chemical shifts against tetramethylsilane (TMS). Electrospray ionization mass spectrometry (ESI-MS) spectra were measured with a LCQ AD (Thermofinnigan, USA) mass spectrometer. The absorption spectra of the dyes in methanol solution and absorbed on the TiO_2 films were measured with a Jasco-550 UV–vis spectrophotometer. The fluorescence spectra of the dyes in methanol solution were observed on a Cary Eclipse fluorescence spectrophotometer at ambient temperature. The oxidation potentials of the dyes in acetonitrile were measured in a three-electrode system with a glassy carbon working electrode, a Pt-wire counter electrode, and a Ag/Ag$^+$ reference electrode which was calibrated with ferrocene [22]. The differential pulse voltammetry (DPV) measurements were performed with a PARSTAT 2273 electrochemical analyzer. The supporting electrolyte was 0.1 M tetrabutylammonium perchlorate (TBAP) in dry acetonitrile, which was purged with argon (99.999%) and stirred for 15 min prior to the scan. Impedance

measurements were also performed with a PARSTAT 2273 electrochemical analyzer with a frequency range of 100 mHz to 100 kHz and a magnitude of 10 mV for modulation signal.

2.3. Computation methods

The geometrical and electronic properties of the TPAR11 and TC12 were performed with the Gaussian 03 program package [23]. The calculation was optimized by means of the B3LYP (Becke three parameters hybrid functional with Lee–Yang–Perdew correlation functionals) with the Pople 6–31 + g(d) atomic basis set. The excitation transitions of TPAR11 and TC12 were calculated using time-dependent density functional theory (TD-DFT) calculations with B3LYP/6–31 + g(d). Molecular orbitals were visualized using Gaussview.

2.4. Cell preparation and photovoltaic characterization

Detailed procedures for the electrode preparation of nanocrystalline TiO_2 films have been reported elsewhere [15,16]. The thickness of the TiO_2 films was obtained by a Wyko NT1100 Optical Profiler (Veeco Metrology Group). The surface area of the TiO_2 electrode was measured by a Microtek scanner with the image integration of 600 dpi resolution. The TiO_2 electrodes were immersed into a dry methanol solution of the dye (standard concentration 3×10^{-4} M) and kept at room temperature for 24 h. The dye-coated electrodes were rinsed quickly with ethanol and the photoelectrochemical measurement was conducted immediately.

The electrochemical cell used for photovoltaic measurements consisted of a dye-adsorbed TiO_2 electrode, a counter-electrode with a thin thermal pyrolysis Pt layer [24], a tape spacer (42 μm thick for the sealing), and an organic electrolyte with a mixture of 0.6 M 1,2-dimethyl-3-propylimidazolium iodide (DMPImI), 0.1 M LiI, and 0.05 M I_2 in acetonitrile. Photoelectrochemical performance of the solar cell was measured using a Keithley 2400 digital source meter controlled by a computer [25]. A 500-W Xe lamp served as the light source in combination with a band-pass filter (400–800 nm) to remove ultraviolet and infrared radiation for giving 100 mW cm^{-2} (the equivalent of one sun) at the surface of the test cell. The incident light intensity was calibrated by a radiometer. Further calibration was carried out by using a USB 4000 plug-and-play miniature fiber optic spectrometer (Ocean Optics Inc., USA) to reduce the mismatch between the simulated and the true solar spectrum.

3. Results and discussion

3.1. Absorption and luminescence properties

Fig. 2 shows the absorption spectra of the dyes in methanol solution. With the same donor part, the shape of the absorption spectra around 350 nm of TPAR11 and TC12 is quite similar, which can be assigned to a π–π* transition. While the absorption band with λ_{max} above 400 nm corresponds to an intramolecular charge transfer (ICT) between the TPA donor part of the molecule and the acceptor end group. The TPAR11 dye with rhodanine-3-acetic acid as the acceptor group shows bathochromic shift in max adsorption bands by 56 nm compared with that of TC12 dye with cyanoacrylic acid as the acceptor part. This shift is owing to that the rhodanine-3-acetic acid extends the π-conjugation system of TPAR11 dye through the 4-oxo-2-thioxothiazolidine ring [26]. As summarized in Table 1, the molar adsorption coefficients for the TPAR11 and TC12 dyes at the λ_{max} in methanol solution are calculated to be 40,000 and 30,000 M^{-1} cm^{-1}, respectively. When the TPAR11 and TC12 dyes are excited within their π–π* bands in an air-equilibrated solution at 298 K, they exhibit strong luminescence maxima at 539 and 479 nm, respectively.

Table 1
Absorption and emission properties of TPAR11 and TC12 dyes

Dye	λ_{max}[a] (nm)	ε_{max}[a] (M^{-1} cm^{-1})	λ_{em}[b] (nm)	Amount[c] ($\times 10^{-8}$ mol cm^{-2})
TPAR11	466	40,000	539	6.9
TC12	410	30,000	479	13.8

[a]Absorption and [b]emission spectra were measured in methanol solution. The emission spectra were obtained with the concentration of 5×10^{-5} M at 293 K. ε_{max} is the extinction coefficient at λ_{max} of absorption. [c]Amount of the dyes absorbed on TiO_2 film.

The amount of dye adsorbed on the TiO_2 film was estimated by desorbing the dye with basic solution, and the results are summarized in Table 1. The adsorbed amount of TPAR11 on the film was 0.069 μmol cm^{-2}, which is just half that of TC12 (0.138 μmol cm^{-2}). This decrease is due to the larger acceptor part of TPAR11. In comparison, with the addition of 1 mM CDCA, the adsorbed amount of TPAR11 and TC12 were 0.059 and 0.130 μmol cm^{-2}, respectively. This change indicates that CDCA molecule occupies the position of dye molecule anchoring to the TiO_2 film with the restraining aggregation of dye molecule.

3.2. Molecular-structure analysis

Fig. 3 shows the schematic representation of the molecular orbital energies for the two as-synthesized dyes in vacuo. Considering the form of dyes anchored onto the TiO_2 surface, the molecular orbital energies of their potassium salts were also represented. Observation of the frontier orbitals of the two dyes in vacuo shows that the HOMO and LUMO are essentially isolated in energy, with the HOMO−1 and LUMO+1 lying ca. 0.7 eV below and above the HOMO and LUMO, respectively. Compared with TC12, TPAR11 with higher HOMO and lower LUMO shows the narrowest HOMO–LUMO gap, which is beneficial for absorbing the long wave light. The higher LUMO of TC12 compared with that of TPAR11 is more evident in their potassium salts calculation. Since the LUMO position affects the photovoltage of DSC partly, the cell based on TC12 may show a higher V_{oc} than that of TPAR11, which will be validated below.

Fig. 4 shows the frontier orbital plots of the HOMO and LUMO of TPAR11 and TC12. The HOMO of either TPAR11 or TC12 is delocalized in a large extent over the entire molecule, indicating that the binding energy of the electrons in the HOMO is sensi-

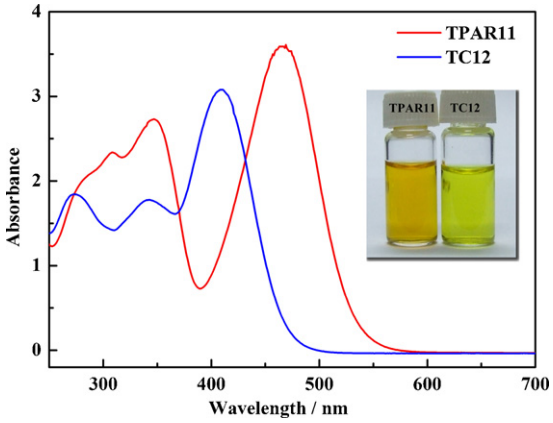

Fig. 2. UV–vis absorption spectra of the TPAR11 and TC12 measured in methanol solution with the concentration of 0.1 mM. Inset photograph shows methanol solution of the two dyes in glass bottles.

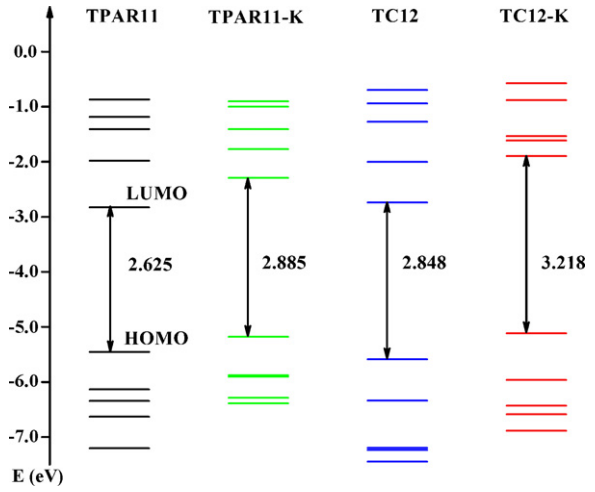

Fig. 3. Schematic representation of the molecular orbital energies of TPAR11 and TC12 with their potassium salts in vacuo.

tive to a change in the π-system [27]. In comparison, the LUMO of TC12 is delocalized over the cyanoacrylic unit through vinyl group, while the LUMO of TPAR11 is delocalized over the 4-oxo-2-thioxothiazolidine ring but the delocalization is broken between the 4-oxo-2-thioxothiazolidine ring and the acetic acid. Examination of the HOMO and LUMO plots of TPAR11 and TC12 indicates that the HOMO to LUMO excitation induced by photo moved the electron distribution from the donor part to the acceptor group, which results in an efficient charge separation. Meanwhile, the collected electron distributions for the occupied states are quite similar for the two dyes, as the dipole moments are comparable, μ = 6.93 D for TPAR11 and μ = 6.87 D for TC12.

To analyze the photophysical properties of the dyes, we also performed TD-DFT calculations of the lowest 10 singlet–singlet excitations of both dyes in methanol solutions that were used as the solvent to record the experimental spectra. Considering the energy range, the three transitions of TPAR11 and TC12 with oscillator strengths (f) above 0.1 are summarized in Table 2. The lowest transition is calculated to be 2.41 and 2.63 eV for TPAR11 and TC12, respectively, corresponding to a charge-transfer excitation of the HOMO to the LUMO. Compared with the experiment data, the considerable red-shift of the absorption maximum from calculation is related to the self-interaction error in TD-DFT arising through the

Table 2
Calculated TD-DFT excitation energies (E), oscillator strengths (f), composition in terms of molecular orbital contributions and character, as compared to the maximum band of experimental absorption

Dye	E (eV) (nm)	f	Composition	Exp. (eV) (nm)
TPAR11	2.41 (514)	1.02	86% HOMO → LUMO	2.66 (466)
	3.04 (408)	0.46	51% HOMO−1 → LUMO	3.57 (347)
	3.22 (385)	0.29	44% HOMO → LUMO+1	
TC12	2.63 (471)	0.83	87% HOMO → LUMO	3.02 (410)
	3.20 (387)	0.45	68% HOMO → LUMO+1	3.62 (342)
	3.45 (359)	0.33	65% HOMO−1 → LUMO	

Table 3
Electrochemical data of the as-synthesized TPAR11 and TC12

Dye	E_{0-0} (eV)	$E(S^+/S)$ (V)	$E(S^+/S^*)$ (V)	E_{gap} (V)
TPAR11	2.47	0.85	−1.62	1.12
TC12	2.79	0.88	−1.91	1.41

The E_{0-0} value was estimated from the cross-section of absorption and emission spectra. The ground-state oxidation potentials $E(S^+/S)$ was measured on 0.1 M tetrabutylammonium perchlorate in acetonitrile using glassy carbon working electrode, Pt counter electrode, and Ag/Ag^+ reference electrode. The excited-state oxidation potential $E(S^+/S^*)$ was calculated from $E(S^+/S)$–E_{0-0}. E_{gap} is the energy gap between the $E(S^+/S^*)$ of the dye and the conduction band level of TiO_2 (−0.5 V vs. NHE).

electron transfer in the extended charge-transfer state [28]. The band experimentally found at 3.57 eV for TPAR11 and 3.62 eV for TC12 appears to be composed of almost overlapping π–π^* transitions of different character. The better agreement between the calculated and experimental absorption energies of the π–π^* features as compared to the charge transfer excitation is related to the localized character of the π–π^* excitations, which involve substantially overlapping orbitals [29].

3.3. Redox behavior

The oxidation potentials of the ground state $E(S^+/S)$ corresponding to the HOMO levels of the dyes were measured by differential pulse voltammetry. As summarized in Table 3, the $E(S^+/S)$ of TPAR11 and TC12 dyes are 0.85 and 0.88 V vs. NHE, respectively. These values are sufficiently more positive than the iodide/triiodide redox potential (~0.45 V vs. NHE) [30], indicating that the oxidized dyes formed after electrons injection into the conduction band of TiO_2 could accept electrons from I^- ions thermodynamically.

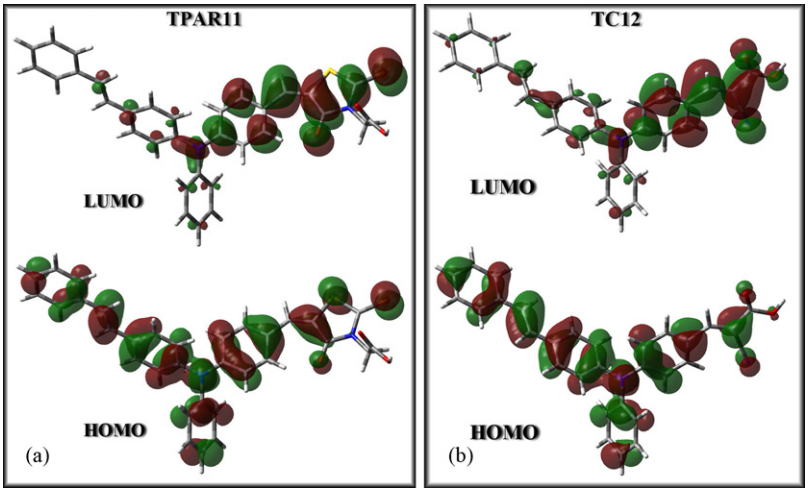

Fig. 4. The frontier orbital plots of the HOMO and LUMO of TPAR11 (a) and TC12 (b).

The excited-state oxidation potentials $E(S^+/S^*)$ of the two as-synthesized dyes, which correspond to the LUMO levels of the dyes and play an important role for the direction prior determination of current flow in the electron injection process, can be extracted from the oxidation potential of the ground state $E(S^+/S)$ and the zero–zero excitation energy E_{0-0} according to

$$E(S^+/S^*) = E(S^+/S) - E_{0-0} \quad (1)$$

As listed in Table 3, the $E(S^+/S^*)$ values of TPAR11 and TC12 are −1.62 and −1.91 V vs. NHE, respectively, which are notably more negative than the equivalent potential of the TiO_2 conduction band edge E_{cb} (−0.5 V vs. NHE) [31]. The energy gap E_{gap} between the $E(S^+/S^*)$ of the dye and the conduction band level of TiO_2 can be derived according to

$$E_{gap} = E_{cb} - E(S^+/S^*) \quad (2)$$

Assuming that the E_{gap} around 0.2 eV is the minimum value for efficient electron injection [13], the E_{gap} listed in Table 3, which were above 0.2 V, indicates that the excited electrons of dye molecules can be injected into the conduction band of TiO_2 thermodynamically. As an increased gap between the conduction band and the redox couple of electrolyte results in a higher open-circuit potential, the present two dyes could be very fascinating for improving the efficiency of DSCs with the anode based on semiconductor materials with Fermi levels more negative than that of titanium dioxide.

3.4. Photovoltaic performance

Fig. 5 shows the incident monochromatic photo-to-current conversion efficiency (IPCE) and the photocurrent density vs. voltage curves of DSCs based on the as-synthesized dyes with or without CDCA addition. The IPCE data of the TPAR11 is red-shifted by about 30 nm as compared to the TC12, which is consistent with the absorption spectra of both dyes. With the addition of CDCA, the IPCE spectrum of TPAR11 gets much higher at the region of 400–500 nm, while the IPCE data of TC12 has no markedly change. The improved IPCE performance of DSCs based on the TPAR11 with CDCA results higher short current density, which will be shown below.

The light-to-electricity conversion efficiency (η) of the DSCs under white-light irradiation can be calculated from the short-circuit photocurrent density (J_{sc}), the open-circuit photovoltage (V_{oc}), the fill factor of the cell (ff), and the intensity of the incident light (P_{in}) from the following equation [32]:

$$\eta(\%) = \frac{J_{sc}\,(\mathrm{mA/cm^2}) \times V_{oc}\,(\mathrm{V}) \times \mathrm{ff}}{P_{in}\,(\mathrm{mW/cm^2})} \times 100 \quad (3)$$

Table 4
Photovoltaic performance of DSCs based on TPAR11 and TC12 with or without the addition of CDCA

Dye	Device	CDCA (mM)	V_{oc} (mV)	J_{sc} (mA cm^{-2})	ff	η (%)
TPAR11	Cell A	0	560	13.5	0.62	4.67
	Cell A_C	1	569	16.1	0.60	5.46
TC12	Cell B	0	638	12.6	0.63	5.05
	Cell B_C	1	734	12.9	0.63	5.96

The detailed parameters (J_{sc}, V_{oc}, ff, and η) are summarized in Table 4. As seen from Table 4, the DSC based on TPAR11 without CDCA (Cell A) gave a short circuit photocurrent density of 13.5 mA cm^{-2}, an open circuit voltage of 560 mV, and a fill factor of 0.62, corresponding to an overall conversion efficiency of 4.67%. By contrast, the TC12 sensitized cell (Cell B) gave a lower J_{sc} (12.6 mA cm^{-2}), but higher V_{oc} (638 mV) and conversion efficiency (5.05%), demonstrating that the higher LUMO level of TC12 potassium salts is beneficial for the increase of the cell voltage and conversion efficiency.

From Table 4, one can also see that the addition of 1 mM CDCA improves the performance of the DSCs. From Cell A to Cell A_C, the obvious improvement is J_{sc}, which was increased from 13.5 to 16.1 mA cm^{-2}. While from Cell B to Cell B_C, the obvious increase is V_{oc}, which was increased from 638 to 734 mV. In both cases, the addition of CDCA improved the efficiency of the DSCs.

3.5. Electrochemical impedance spectroscopy (EIS) studies

Electrochemical impedance spectroscopy has been widely used to study the kinetics of electrochemical processes including the illustration of transferred electronic and ionic processes occurring in the DSC [33]. Fig. 6a shows the typical EIS spectrum of DSC at several bias voltages presented in the form of Nyquist plots. The larger semicircle at lower frequencies is attributed to the charge-transfer at the TiO_2/electrolyte interface and the ion diffusion of redox species in the electrolyte. Fitting the low-frequency semicircle with the equivalent circuit shown in Fig. 6b subsequently gives the charge-transfer resistance (R_{ct}, Fig. 6c) and the chemical capacitance (C_μ, Fig. 6d) at the TiO_2/electrolyte interface.

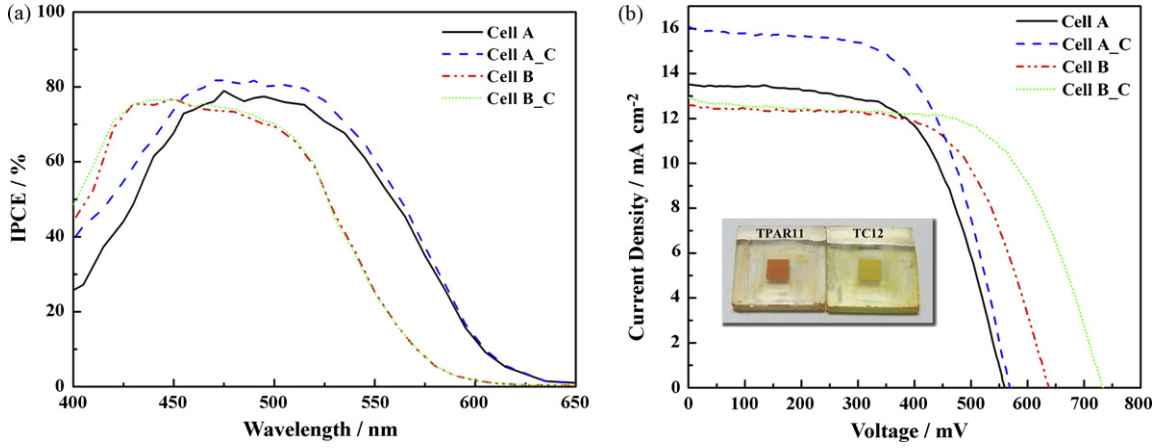

Fig. 5. IPCE spectrum (a) and photocurrent density–voltage characteristics (b) for the cells based on TPAR11 (Cell A), TPAR11 + 1 mM CDCA (Cell A_C), TC12 (Cell B), TC12 + 1 mM CDCA (Cell B_C). Inset photo of (b) shows the dye-adsorbed TiO_2 films used in the photovoltaic characterization.

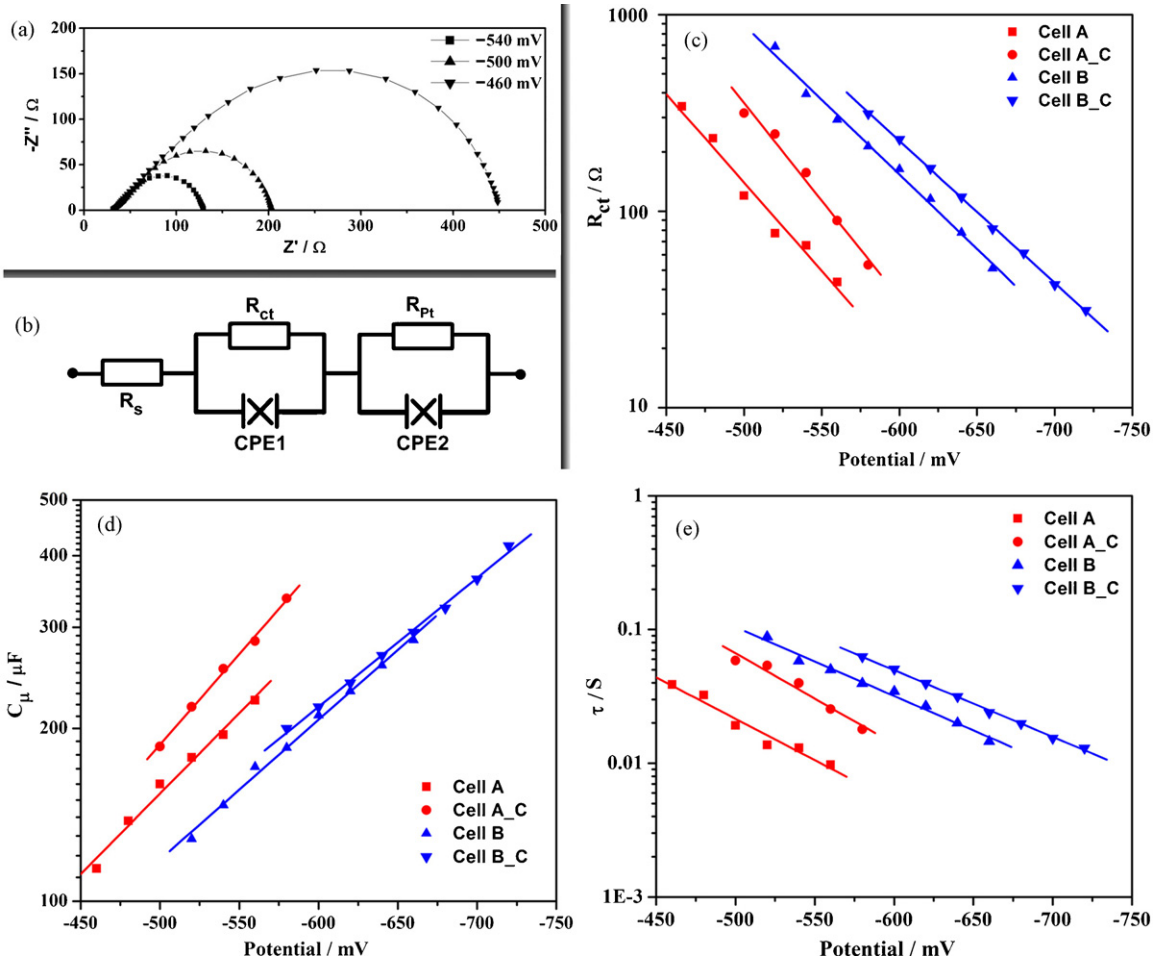

Fig. 6. (a) Electrochemical impedance spectra of the cell based on TPAR11 at several forward bias near the open-circuit potential in the dark and (b) the equivalent circuit of the cells. The fitting results are plotted as (c) charge-transfer resistance R_{ct}, (d) film capacitance C_μ, and (e) electron lifetime with respect to the externally controlled potentials.

R_{ct} follows the Buttler–Volmer relationship that yields to [34]

$$R_{ct} = R_0 \exp\left[-\frac{e\beta}{kT}(E_F - E_r)\right] \quad (4)$$

where E_F is the position of the Fermi level of electrons, E_r is the position of the redox couple,$-(E_F - E_r)$ is the applied potential at the electrode, e is the electron charge, β is the transfer coefficient, R_0 is a constant, k is the Boltzman constant, and T is the absolute temperature. As shown in Fig. 6c, the R_{ct} decreases as the applied potentials become more negative. At a given potential, Cell A has the lowest R_{ct}, which means the highest charge losses in the TiO_2/electrolyte interface. As the larger charge losses limit the open circuit potential to lower values, Cell A shows the lowest V_{oc}. By contrast, Cell B_C with the highest R_{ct} shows the highest V_{oc}.

From Fig. 6d, one can see that C_μ follows a characteristic exponential rise with increasing forward bias. This behavior is generally analyzed to yield the chemical capacitance of nanostructured TiO_2 by using the following model [35]:

$$C_\mu = \frac{e^2}{kT} \exp\left[\frac{\alpha e}{kT}(E_F - E_{cb})\right] \quad (5)$$

where E_{cb} is the position of the conduction band and α is a constant related to the distribution of electronic states below the conduction band. The much higher capacitance indicates a higher density of accessible electronic states at the surface. As shown in the model above, part of this capacity increase is thus caused by the negative shift in the conduction band position, which agrees with the larger short circuit current observed with these cells. As a result, Cell A_C with the largest C_μ shows the highest J_{sc}, and Cell B with the lowest C_μ shows the lowest J_{sc}.

The influence of CDCA on the photovoltaic performance of the dyes with different acceptor moieties is the collective effects of both R_{ct} and C_μ. As shown in Fig. 6c, R_{ct} of cells with CDCA is universally higher than that of the corresponding cells without CDCA at a given applied potential. This result means that the coadsorbent CDCA shifts the Fermi level of semiconductor film to a more negative position, which increases the open-circuit photovoltage of DSCs. The reason for the improved V_{oc} with CDCA addition in TC12 rather in TPAR11 is still being researched. On the other hand, the electron delocalization of TPAR11 is broken between the 4-oxo-2-thioxothiazolidine ring and the acetic acid, which have been discussed before. This will make the photo-excited electrons difficult to reach the TiO_2 film, and easy to quench between molecules. This process is the main factor limiting the photocurrent. As CDCA can avoid these unwanted phenomena efficiently, the J_{sc} of the cells based on TPAR11 increase much higher than that of TC12.

The product of the R_{ct} and C_μ corresponds to the electron lifetime τ, as shown in Fig. 6e. The increase in τ is associated with a pronounced rise in the charge-transfer resistance, indicating that the cografting of CDCA decreases the interfacial rate constant for electron capture by triiodide ions. It is interesting that Cell B_C presents a slightly longer electron lifetime than that of the oth-

ers. This is one of the reasons why its photovoltaic performance is superior to those of others.

4. Conclusions

Two triphenylamine-based organic dyes with different acceptors (TPAR11 and TC12) showed the different photovoltaic performance. Theoretical calculation shows that the delocalization of the excited state for TPAR11 is broken between the 4-oxo-2-thioxothiazolidine ring and the acetic acid. The cells sensitized by TPAR11 displayed a higher photocurrent, while the cells sensitized by TC12 showed a higher photovoltage. The analysis of the electrochemical impedance spectroscopy of the DSCs reveals that the position of Fermi level of electron in the TiO_2 films plays a dominant role in the change of accumulation and recombination. It is found that by the addition of 1 mM CDCA coadsorbent, the DSCs based on TPAR11 and TC12 showed the light-to-electricity conversion efficiency of 5.46% and 5.96%, respectively. The high efficiency of the DSCs in this study is ascribed to the low recombination rate and long lifetime of electrons in TiO_2. As CDCA has different effect on dyes with different acceptor moiety, this study also draws attention to the possibility of enhancing the photovoltaic performance by developing coadsorbents that not only shift the band edges of TiO_2 to negative potentials but also shield its surface against recombination.

Acknowledgements

This work was supported by the Research Programs from the National MOST (2005CB623607) and Tianjin City (07ZCGHHZ00700 and 08JCZDJC21300). We acknowledge the computational support by NKSTARS provided by the Center of Theoretical and Computational Chemistry at Nankai University.

References

[1] M. Grätzel, Nature 414 (2001) 334–338.
[2] Q.B. Meng, K. Takahashi, X.T. Zhang, I. Sutanto, T.N. Rao, O. Sato, A. Fujishima, H. Watanabe, T. Nakamori, M. Uragami, Langmuir 19 (2003) 3572–3574.
[3] C.W. Shi, S.Y. Dai, K.J. Wang, X. Pan, L. Guo, L.Y. Zeng, L.H. Hu, F.T. Kong, Sol. Energy Mater. Sol. Cells 86 (2005) 527–535.
[4] Z.G. Chen, Y.W. Tang, H. Yang, Y.Y. Xia, F.Y. Li, T. Yi, C.H. Huang, J. Power Sources 171 (2007) 990–998.
[5] J.H. Wu, Z. Lan, J.M. Lin, M.L. Huang, P.J. Li, J. Power Sources 173 (2007) 585–591.
[6] M. Grätzel, Inorg. Chem. 44 (2005) 6841–6851.
[7] Z.S. Wang, K. Hara, Y. Dan-oh, C. Kasada, A. Shinpo, S. Suga, H. Arakawa, H. Sugihara, J. Phys. Chem. B 109 (2005) 3907–3914.
[8] http://kuroppe.tagen.tohoku.ac.jp/~dsc/cell-e.htm.
[9] T. Kitamura, M. Ikeda, K. Shigaki, T. Inoue, N.A. Anderson, X. Ai, T.Q. Lian, S. Yanagida, Chem. Mater. 16 (2004) 1806–1812.
[10] D.P. Hagberg, T. Edvinsson, T. Marinado, G. Boschloo, A. Hagfeldt, L.C. Sun, Chem. Commun. (2006) 2245–2247.
[11] V. Shklover, Y.E. Ovchinnikov, L.S. Braginsky, S.M. Zakeeruddin, M. Grätzel, Chem. Mater. 10 (1998) 2533–2541.
[12] S. Ito, S.M. Zakeeruddin, R. Humphry-Baker, P. Liska, R. Charvet, P. Comte, M.K. Nazeeruddin, P. Péchy, M. Takata, H. Miura, S. Uchida, M. Grätzel, Adv. Mater. 18 (2006) 1202–1205.
[13] K. Hara, T. Sato, R. Katoh, A. Furube, Y. Ohga, A. Shinpo, S. Suga, K. Sayama, H. Sugihara, H. Arakawa, J. Phys. Chem. B 107 (2003) 597–606.
[14] K. Hara, M. Kurashige, Y. Dan-oh, C. Kasada, A. Shinpo, S. Suga, K. Sayama, H. Arakawa, New J. Chem. (2003) 783–785.
[15] M. Liang, W. Xu, F.S. Cai, P. Chen, B. Peng, J. Chen, Z.M. Li, J. Phys. Chem. C 111 (2007) 4465–4472.
[16] W. Xu, B. Peng, J. Chen, M. Liang, F.S. Cai, J. Phys. Chem. C 112 (2008) 874–880.
[17] E. Palomares, J.N. Clifford, S.A. Haque, T. Lutz, J.R. Durrant, J. Am. Chem. Soc. 125 (2003) 475–482.
[18] G. Schlichthörl, S.Y. Huang, J. Sprague, A.J. Frank, J. Phys. Chem. B 101 (1997) 8141–8155.
[19] K. Hara, Y. Dan-oh, C. Kasada, Y. Ohga, A. Shinpo, S. Suga, K. Sayama, H. Arakawa, Langmuir 20 (2004) 4205–4210.
[20] T. Horiuchi, H. Miura, K. Sumioka, S. Uchida, J. Am. Chem. Soc. 126 (2004) 12218–12219.
[21] G.F. Lai, X.R. Bu, J. Santos, E.A. Mintz, Synlett 11 (1997) 1275–1276.
[22] R.R. Gagné, C.A. Koval, G.C. Lisensky, Inorg. Chem. 19 (1980) 2854–2855.
[23] M.J. Frisch, G.W. Trucks, H.B. Schlegel, G.E. Scuseria, M.A. Robb, J.R. Cheeseman Jr., J.A. Montgomery, T. Vreven, K.N. Kudin, J.C. Burant, J.M. Millam, S.S. Iyengar, J. Tomasi, V. Barone, B. Mennucci, M. Cossi, G. Scalmani, N. Rega, G.A. Petersson, H. Nakatsuji, M. Hada, M. Ehara, K. Toyota, R. Fukuda, J. Hasegawa, M. Ishida, T. Nakajima, Y. Honda, O. Kitao, H. Nakai, M. Klene, X. Li, J.E. Knox, H.P. Hratchian, J.B. Cross, C. Adamo, J. Jaramillo, R. Gomperts, R.E. Stratmann, O. Yazyev, A.J. Austin, R. Cammi, C. Pomelli, J.W. Ochterski, P.Y. Ayala, K. Morokuma, G.A. Voth, P. Salvador, J.J. Dannenberg, V.G. Zakrzewski, S. Dapprich, A.D. Daniels, M.C. Strain, O. Farkas, D.K. Malick, A.D. Rabuck, K. Raghavachari, J.B. Foresman, J.V. Ortiz, Q. Cui, A.G. Baboul, S. Clifford, J. Cioslowski, B.B. Stefanov, G. Liu, A. Liashenko, P. Piskorz, I. Komaromi, R.L. Martin, D.J. Fox, T. Keith, M.A. Al-Laham, C.Y. Peng, A. Nanayakkara, M. Challacombe, P.M.W. Gill, B. Johnson, W. Chen, M.W. Wong, C. Gonzalez, J.A. Pople, Gaussian 03, Revision C.01 Gaussian, Inc., Wallingford, CT, 2004.
[24] F.J. Li, F.Y. Cheng, J.F. Shi, F.S. Cai, M. Liang, J. Chen, J. Power Sources 165 (2007) 911–915.
[25] F.S. Cai, J. Chen, R.S. Xu, Chem. Lett. 35 (2006) 1266–1267.
[26] D. Kim, J.K. Lee, S.O. Kang, J. Ko, Tetrahedron 63 (2007) 1913–1922.
[27] P. Qin, X. Yang, R. Chen, L. Sun, T. Marinado, T. Edvinsson, G. Boschloo, A. Hagfeldt, J. Phys. Chem. C 111 (2007) 1853–1861.
[28] A. Dreuw, M. Head-Gordon, J. Am. Chem. Soc. 126 (2004) 4007–4016.
[29] S. Kim, J.K. Lee, S.O. Kang, J. Ko, J.H. Yum, S. Fantacci, D.A. Filippo, D.D. Censo, M.K. Nazeeruddin, M. Grätzel, J. Am. Chem. Soc. 128 (2006) 16701–16707.
[30] G. Smestad, Sol. Energy Mater. Sol. Cells 32 (1994) 273–288.
[31] A. Hagfeldt, M. Grätzel, Chem. Rev. 95 (1995) 49–68.
[32] A. Hagfeldt, M. Grätzel, Acc. Chem. Res. 33 (2000) 269–277.
[33] F. Fabregat-Santiago, J. Bisquert, G. Garcia-Belmonte, G. Boschloo, A. Hagfeldt, Sol. Energy Mater. Sol. Cells 87 (2005) 117–131.
[34] Q. Wang, S. Ito, M. Grätzel, F. Fabregat-Santiago, I. Mora-Seró, J. Bisquert, T. Bossho, H. Imai, J. Phys. Chem. B 110 (2006) 25210–25222.
[35] J. Bisquert, Phys. Chem. Chem. Phys. 5 (2003) 5360–5364.